
Neural Architecture Generator Optimization

Binxin Ru¹ Pedro Esperanca² Fabio Carlucci²

Abstract

Neural Architecture Search (NAS) was first proposed to achieve state-of-the-art performance through the discovery of new architecture patterns, without human intervention. An over-reliance on expert knowledge in the search space design has however led to increased performance (local optima) without significant architectural breakthroughs, thus preventing truly novel solutions from being reached. In this work we propose 1) to cast NAS as a problem of finding the optimal network generator and 2) a new, hierarchical and graph-based search space capable of representing an extremely large variety of network types, yet only requiring few continuous hyper-parameters. This greatly reduces the dimensionality of the problem, enabling the effective use of Bayesian Optimisation as a search strategy. At the same time, we expand the range of valid architectures, motivating a multi-objective learning approach. We demonstrate the effectiveness of our strategy on six benchmark datasets and show that our search space generates extremely lightweight yet highly competitive models illustrating the benefits of a NAS approach that optimises over network generator selection.

1. Introduction

Neural Architecture Search (NAS) has the potential to discover paradigm-changing architectures with state-of-the-art performance, and at the same time removes the need for a human expert in the network design process. While significant improvements have been recently achieved (Liu et al., 2019; Chen et al., 2019; Pham et al., 2018; Carlucci et al., 2019; Li et al., 2019; Cai et al., 2019), this has taught us little about *why* a specific architecture is more suited for a given dataset. Similarly, no conceptually new architecture

This work was done when Binxin Ru was a research intern at Huawei Noah’s Ark Lab, London. ¹Machine Learning Research Group, University of Oxford ²Huawei Noah’s Ark Lab, London. Correspondence to: Binxin Ru <robin@robots.ox.ac.uk>, Fabio Carlucci <fabio.maría.carlucci@huawei.com>.

Preprint. Under review

structure has emerged from NAS works. We attribute this to two main issues: (i) reliance on over-engineered search spaces and (ii) the inherent difficulty in analyzing complex architectures.

The first point is investigated in Yang et al. (2020). In order to reduce search time, current NAS methods often restrict the macro-structure and search only the micro-structure at the cell level, focusing on which operations to choose but fixing the global wiring pattern (Liu et al., 2019; Nayman et al., 2019; Fang et al., 2020; Mei et al., 2020). This leads to high task accuracy but restricts the search to local minima of possible architectures: indeed deep learning success stories, such as ResNet (He et al., 2016), DenseNet (Huang et al., 2017) and Inception (Szegedy et al., 2015) all rely on specific global wiring rather than specific operations.

The second issue appears hard to solve, as analyzing the structure of complex networks is itself a demanding task for which few tools are available. We suggest that by moving the focus towards *network generators* we can obtain a much more informative solution, as the whole network can then be represented by a small set of parameters. This idea, first introduced by Xie et al. (2019), offers many advantages for NAS: the smaller number of parameters is easier to optimize and easier to interpret, compared to the popular categorical, high-dimensional search spaces. Furthermore it allows the algorithm to focus on macro differences (e.g. networks belonging to different distributions) and ignore the micro differences arising from minor variations with little impact on the final accuracy.

To summarize, our main contributions are as follows.

- 1) A new **hierarchical, graph-based search space**, together with a stochastic network generator which can output an extremely wide range of previously unseen networks in terms of wiring complexity, memory usage and training time.
- 2) A **Network Architecture Generator Optimization framework** (NAGO), which uses Bayesian Optimization to efficiently explore this search space in both multi-fidelity and multi-objective settings.
- 3) **Extensive empirical evaluation** showing that NAGO achieves state-of-the-art NAS results on a variety of vision tasks, and finds lightweight yet competitive architectures.

2. Related Work

Neural Architecture Search (NAS). NAS aims to automate the design of deep neural networks and was initially formulated as a search problem over the possible operations (e.g. convolutions and pooling filters) in a graph. Several approaches have been proposed that outperform human-designed networks in vision tasks: reinforcement learning (Zoph & Le, 2017; Pham et al., 2018), evolution (Real et al., 2017), gradient descent (Liu et al., 2019; Nayman et al., 2019) and multi-agent learning (Carlucci et al., 2019). To achieve a computationally feasible solution, these works rely on a manually-designed, cell-based search space where the macro-structure of the network (the global *wiring*) is fixed and only the micro-structure (the *operations*) is searched.

Network Wiring. Recent works have explored the importance of the wiring of a network graph. Yuan et al. (2020) use a gradient-based approach to search the network wiring explicitly via learnable weights, Wortsman et al. (2019) search for network wirings using channel instead of layer connections; both modify existing network architectures instead of discovering new ones. Xie et al. (2019) studied CNNs generated from network generators based on random graphs; they show that, even without optimization—either at the micro or macro level—these networks can outperform many traditional NAS methods on image recognition tasks.

Bayesian Optimization. BO is a technique for optimizing a black-box function which is usually noisy and expensive to evaluate. The two key components of BO are: a statistical surrogate model which models the unknown objective; and an acquisition function which is optimized to recommend the next query location by trading off exploration and exploitation (Brochu et al., 2010; Shahriari et al., 2015). BO has been widely used for optimizing the hyperparameters of machine learning algorithms (Snoek et al., 2012; Bergstra et al., 2011; 2013; Hutter et al., 2011; Klein et al., 2016; Falkner et al., 2018; Chen et al., 2018) and more recently it has found applications in NAS (Kandasamy et al., 2018; Ying et al., 2019; Ma et al., 2019; Shi et al., 2019; White et al., 2019). However, current NAS search spaces—even cell-based ones—are noncontinuous and relatively high dimensional (Elsken et al., 2018), thus unfavourable to conventional BO algorithms that focus on low-dimensional continuous problems (Shahriari et al., 2015; Hennig et al., 2015). Thus, to the best of our knowledge, all the existing BO-based NAS approaches only demonstrate their performance on small networks/cells for small image datasets.

3. Neural Architecture Generator

Previous research has shown that small perturbations in the network’s structure do not significantly change its performance, i.e. the specific connection between any single pair

of nodes is less important than the overall connectivity (Xie et al., 2019; Yang et al., 2020). As such, we hypothesize, and experimentally confirm in Section 4.1, that architectures sampled from the same generative distribution perform similarly. This assumption allows us to greatly simplify the search and explore more configurations in the search space by only evaluating those sampled from different generator hyperparameters. Therefore, instead of optimizing a specific architecture, we focus on finding the optimal hyperparameters for a stochastic network generator (see Xie et al. 2019 for an in-depth description of this concept).

3.1. Hierarchical Graph-based Search Space (HNAG)

Our network search space is modelled as a hierarchical graph with three levels (Figure 1). At the top-level, we have a graph of cells. Each cell is itself represented by a mid-level graph. Similarly, each node in a cell is a graph of basic operations (conv 3×3 , conv 5×5 , etc.). This results in 3 sets of graph hyperparameters: θ_{top} , θ_{mid} , θ_{bottom} , each of which independently defines the graph generation model in each level. Following Xie et al. (2019) we use the Watts-Strogatz (WS) model as the random graph generator for the top and bottom levels, with hyperparameters $\theta_{top} = [N_t, K_t, P_t]$ and $\theta_{bottom} = [N_b, K_b, P_b]$; and use the Erdős-Renyi (ER) graph generator for the middle level, with hyperparameters $\theta_{mid} = [N_m, P_m]$, to allow for the single-node case.

By varying the graph generator hyperparameters and thus the connectivity properties at each level, we can produce a extremely diverse range of architectures (see the end of this section). For instance, if the top-level graph has 20 nodes arranged in a feed-forward configuration and the mid-level graph has a single node, then we obtain networks similar to those sampled from the DARTS search space (Liu et al., 2019). While if we fix the top-level graph to 3 nodes, the middle level to 1 and the bottom-level graph to 32, we can reproduce the search space from Xie et al. (2019).

Stages. CNNs are traditionally divided into stages, each having a different image resolution and number of channels (Szegedy et al., 2017; Liu et al., 2019; Xie et al., 2019). In previous works, both the length of each stage and the number of channels were fixed. Our search space is the first that permits the learning of the optimal channel ratio as well as the channel multiplier for each stage. To do so, we define two hyperparameter vectors: stage ratio θ_S and channel ratio θ_C . θ_S is normalized and represents the relative length of each stage. For example, if there are 20 nodes at the top level and $\theta_S = [0.2, 0.2, 0.6]$ then the three stages will have 4, 4 and 6 nodes, respectively. θ_C controls the number of channels in each stage; e.g. if it is set to $[4, 1, 4]$ than stages 1 and 3 hold the same number of channels while stage 2 only holds one fourth of that. The absolute number of channels depends on the overall desired number of parameters while

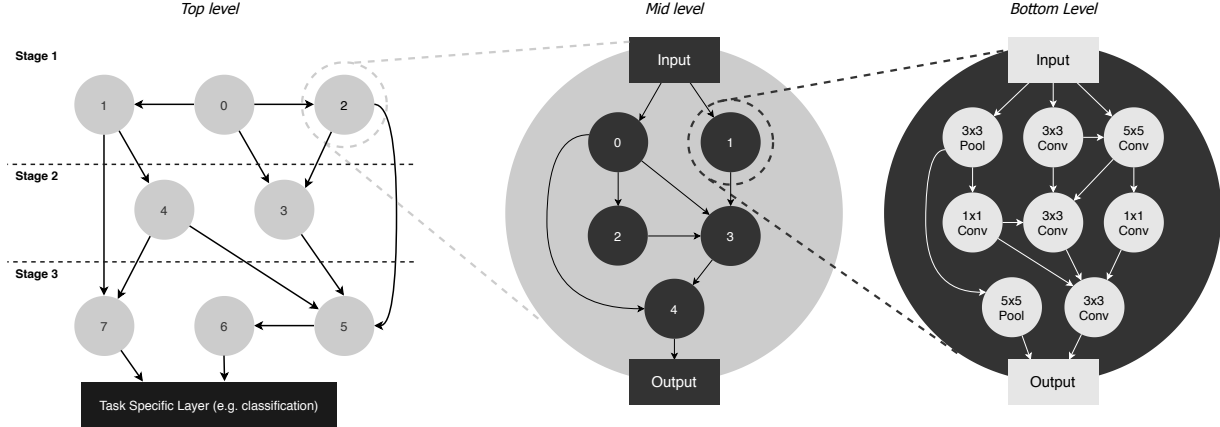


Figure 1. Architecture sampled from HNAG, given hyperparameters Θ . Each node, both in the top-level and mid-level graphs, is an independently sampled graph. Finally, at the bottom level each node corresponds to an independently sampled atomic operation. Note how features at the top level can flow between different stages (e.g. from node 1 and 4 to 7), which could prove beneficial for certain tasks.

θ_C only controls the relative ratio.

Merging options and Operations. When multiple edges enter the same node, they are merged. Firstly, all activations are downsampled via pooling to match the resolution of the smallest tensor. Likewise, we use 1×1 convolutions to ensure that all inputs share the same number of channels. Then, independently for each node, we sample, according to the probability weights θ_M , one merging strategy from: weighted sum, attention weighted sum, concatenation.

Each atomic operation is sampled from a categorical distribution parameterized with θ_{op} , which can be task specific.

Therefore, our search space is fully specified by the hyperparameters $\Theta = [\theta_{top}, \theta_{mid}, \theta_{bottom}, \theta_S, \theta_C, \theta_M, \theta_{op}]$. The top-level enables a mixture of short- and long-range connections among features of different stages (resolutions/channels). The mid-level regulates the search complexity of the bottom-level graph by connecting features computed locally (within each mid-level node).¹ This serves a function similar to the use of cells in other NAS method but relaxes the requirement of equal cells. Our hierarchical search expresses a wide variety of networks (see Section 4.1). The total number of networks in our search space is larger than 4.58×10^{56} . For the DARTS search space that number is $8^{14} \approx 4.40 \times 10^{12}$ (details in Appendix A).

3.2. BO-based Search Strategy

Our proposed hierarchical graph-based search space allows us to represent a wide variety of neural architectures with a small number of continuous hyperparameters, making NAS

¹For example, a 32-nodes graph has 496 possible connections. If we divide this into 4 subgraphs of 8 nodes, that number is $118 = 28 \times 4$ (within subgraphs) + 6 (between subgraphs).

Algorithm 1 BO-based Network Generator Optimization

```

1: Input: Dataset  $K$ , Network generator  $G$ , BO surrogate
   model  $p(f|\Theta, D)$  and acquisition function  $\alpha(\Theta|D)$ 
2: for  $t = 1$  to  $T$  do
3:   Recommend  $\{\Theta_t^j\}_{j=1}^B = \arg \max \alpha_{t-1}(\Theta|D)$ 
4:   for  $j = 1$  to  $B$  in parallel do
5:     Generate a sample architecture from  $G(\Theta_t^j)$ , train
        it on  $K$  and obtain its validation performance  $f_t^j$ 
6:   end for
7:   Update  $D$  and thus  $p(f|\Theta, D)$  with  $\{\Theta_t^j, f_t^j\}_{j=1}^B$ 
8: end for
9: Obtain the best performing  $\Theta^*$  or the Pareto set  $\Theta^*$ 
10: Sample 8 architectures from  $G(\Theta^*)$ , train them to completion and report their test performance.

```

amenable to a wide range of powerful BO methods such as multi-fidelity and multi-objective BO.

3.2.1. MULTI-FIDELITY BO (BOHB)

We use the multi-fidelity BOHB approach, which combines BO with Hyperband to effectively speed up optimization (Falkner et al., 2018). BOHB uses partial evaluations with smaller-than-full budget in order to exclude bad configurations early in the search process, thus saving resources to evaluate more promising configurations. Given the same time constraint, BOHB evaluates many more configurations than conventional BO which evaluates all configurations with full budget.

3.2.2. MULTI-OBJECTIVE BO (MOBO)

We use MOBO to optimize for multiple objectives which are conflicting in nature. For example, we may want to find architectures which give high accuracy but require low mem-

ory; or given a time constraint, we want to find architectures which give high accuracy but are also quick to train.

Given the competing nature of the multiple objectives, we adapt a state-of-the-art MOBO method to learn the Pareto front (Belakaria et al., 2020). The method constructs multiple acquisition functions, one for each objective function, and then recommends the next query point by sampling the point with the highest uncertainty on the Pareto front of all the acquisition functions. We modify the approach in the following two aspects for our application:

Heteroscedastic surrogate model. We use a stochastic gradient Hamiltonian Monte Carlo (SGHMC) BNN (Springenberg et al., 2016), which does a more Bayesian treatment of the weights and thus gives better-calibrated uncertainty estimates than other alternatives in prior BO-NAS works.² SGHMC BNN in (Springenberg et al., 2016) assumes homoscedastic aleatoric noise with zero mean and constant variance w_n^2 . By sampling the network weights w_f and the noise parameter w_n with SGHMC from its posterior $w^i \sim p(w|D)$ where $w = [w_f, w_n]$ conditioned on the training data D for the BNN, the predictive posterior of the BNN is approximated by:

$$\begin{aligned} p(f|\Theta, D) &= \int p(f|\Theta, w)p(w|D)dw = \frac{1}{N} \sum_{i=1}^N p(f|\Theta, w^i) \\ &= \frac{1}{N} \sum_{i=1}^N \mathcal{N} \left(\hat{f}(\Theta; w_f^i), (w_n^i)^2 \right) \end{aligned} \quad (1)$$

The predictive posterior mean $\mu(f|\Theta, D)$ and variance $\sigma^2(f|\Theta, D)$ are computed as:

$$\mu(f|\Theta, D) = \frac{1}{N} \sum_{i=1}^N \hat{f}(\Theta; w_f^i), \quad (2)$$

$$\sigma^2(f|\Theta, D) = \frac{1}{N} \sum_{i=1}^N \hat{f}(\Theta; w_f^i) - \mu(f|D)^2 + w_n^2 \quad (3)$$

However, our optimization problem has heteroscedastic aleatoric noise: the variance in the network performance, in terms of test accuracy or other objectives, depends on the generator hyperparameters (Figure 2). Therefore, we propose to append a second output to the surrogate network and model the noise variance as a deterministic function of the inputs, $w_n^2(\Theta)$. Our heteroscedastic BNN has the same predictive posterior mean as Equation (2) but a slightly different predictive posterior variance:

$$\sigma^2(f|\Theta, D) = \frac{1}{N} \sum_{i=1}^N \left(\hat{f}(\Theta; w_f^i) + (w_n^i(\Theta))^2 \right) - \mu(f|\Theta, D)^2$$

²Ma et al. (2019); Shi et al. (2019) uses a graph neural networks but replacing the final layer with a Bayesian linear regression layer to obtain uncertainty estimates while White et al. (2019) trains a small ensemble of five fully-connected neural networks to approximate the epistemic uncertainties.

Table 1. Regression performance of heteroscedastic (Het) and homoscedastic (Hom) BNN surrogates, trained on 50 generator samples and tested on 100 samples, in terms of negative log-likelihood (NLL) and root mean square error (RMSE)

	NLL		RMSE	
	Hom	Het	Hom	Het
CIFAR10	5.92	3.43	0.02	0.01
CIFAR100	7.15	0.89	0.02	0.02
SPORT8	23.8	19.0	0.15	0.14
MIT67	7.23	-0.92	0.12	0.11
FLOWERS102	15.6	7.49	0.19	0.18

Our resultant surrogate network comprises 3 fully-connected layers, each with 10 neurons, and two outputs. The hyperparameter details for our BNN surrogate is described in Appendix B.

We verify the modelling performance of our heteroscedastic surrogate network by comparing it to its homoscedastic counterpart. We randomly sample 150 points from BOHB query data for each of the five image datasets and randomly split them into a train-test ratio of 1:2. The median results on negative log likelihood (NLL) and root mean square error (RMSE) over 10 random splits are shown in Table 1. The heteroscedastic model not only improves over the homoscedastic model on RMSE, which depends on the predictive posterior mean only, but more importantly, shows much lower NLL, which depends on both the predictive posterior mean and variance. This shows that the heteroscedastic surrogate can model the variance of the objective function better, which is important for the BO exploration.

Despite the superiority in uncertainty estimates, one limitation of SGHMC is that it's not scalable to large networks with large number of parameters. Our low-dimensional search space enables us to use a small network as the surrogate and thus enable the efficient use of SGHMC.

Parallel evaluations per BO iteration The original multi-objective BO algorithm is sequential (i.e. recommends one new configuration per iteration). We modify the method to a batch algorithm which recommends multiple new configurations per iteration and enjoys faster convergence in terms of BO iterations (González et al., 2016; Alvi et al., 2019). This allows the use of parallel computation to evaluate batches of configurations simultaneously. We collect the batch by applying the local penalisation on the uncertainty metric of the original multi-objective BO (Alvi et al., 2019). See Appendix C for details.

4. Experiments

We experiment with the following two network generators.

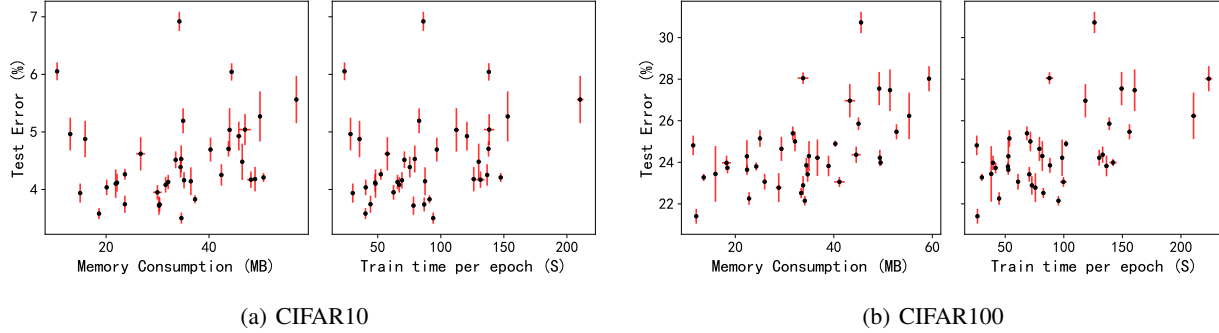


Figure 2. Expressiveness of our HNAG search space. The above plots shows the mean and standard deviation of test error vs. memory consumption and training time per epoch achieved by 40 random generator hyperparameters for CIFAR10 and CIFAR100. The mean and standard deviation of results over the 8 sampled architectures for each generator hyperparameter are presented.

1) Hierarchical Neural Architecture Generator (**HNAG**): our proposed 3-level, hierarchical generator. Due to resource constraint, we limit our search space to the 8 random graph generator hyperparameters $[\theta_{top}, \theta_{mid}, \theta_{bottom}]$, namely the 3 WS graph hyperparameters at top and bottom levels, $\theta_{top} \in \mathbb{R}^3, \theta_{bottom} \in \mathbb{R}^3$; and the 2 ER graph hyperparameters at mid level, $\theta_{mid} \in \mathbb{R}^2$. The search ranges of these hyperparameters are in Appendix D. Following Xie et al. (2019) we fix $\theta_S = [0.33, 0.33, 0.33]$ and $\theta_C = [1 : 2 : 4]$. The absolute number of channels for each stage is computed by multiplying the channel ratio with a constant which is calculated based on our parameter limit.

2) Randomly Wired Neural Architecture Generator (**RNAG**): the 3-stage network generator proposed in Xie et al. (2019) which uses one WS graph for each stage. We optimize the three WS hyperparameters (N, K, P) for each stage, leading to 9 hyperparameters in total.

For both HNAG and RNAG, we apply multi-fidelity and multi-objective BO to optimize their hyperparameters, leading to 4 methods for comparison: HNAG-BOHB, HNAG-MOBO, RNAG-BOHB, RNAG-MOBO. To verify the effectiveness of our search strategy as well as expressiveness, we also evaluate the performance of random samples drawn from HNAG (HNAG-RS) and use it as another baseline. For all generator-based methods, we use summation to merge the inputs and only use 3×3 convolution as the operation choice, unless otherwise stated.

Datasets. We perform experiments on a variety of image datasets: CIFAR10, CIFAR100 (Krizhevsky, 2009), IMAGENET (Deng et al., 2009) for object recognition; SPORT8 for action recognition (Li & Fei-Fei, 2007); MIT67 for scene recognition (Quattoni & Torralba, 2009); FLOWERS102 for fine-grained object recognition (Nilsback & Zisserman, 2008). We limit the number of network parameters to 4.0M for small-image tasks and 6.0M for large-image tasks.

Complete training protocol. For all datasets except IMAGENET, we evaluate the performance of the (Pareto) optimal generators recommended by BO by sampling 8 networks from the generator and training them to completion (600 epochs) with initial learning rate 0.025 and batch size 96. For IMAGENET, we follow the complete training protocol of small model regime in Xie et al. (2019), which trains the networks for 250 epochs with an initial learning rate of 0.1 and a batch size of 256. We use cutout with length 16 for small-image tasks and size 112 for large-image tasks. All experiments use NVIDIA Tesla V100 GPUs.

4.1. Expressiveness of the search space

We evaluate the performance of 40 randomly sampled network generator hyperparameters for CIFAR10 and CIFAR100 (Figure 2). The performance of each hyperparameter set is evaluated by training 8 neural network architectures generated by following the complete training protocol (described above) and evaluating on the test datasets. There are three observations we highlight.

Firstly, the accuracy (test error) and efficiency (memory consumption³ or training time) achieved by different generator hyperparameters are spread over a considerable range. This shows that our search space can express a variety of generators whose networks have different characteristics, thus optimization is meaningful.

Secondly, the networks produced by good generator hyperparameters mostly have small variation in their accuracy and memory, which justifies our proposal to focus on the generator instead of the network. It also supports our approach to assess the performance of a specific generator configuration with only one architecture sample in our BO phase.

Third, there exist Pareto optimal generator hyperparameters

³See Appendix E for a comparison with DARTS search space.

Table 2. Validation accuracy (%) and search cost (GPU days) for BOHB results. The accuracy reported is obtained in the BOHB search setting which uses large batch sizes based on GPU machine memory and trains the network sample for 400 epochs for SPORT8 and 120 epochs for the other datasets.

	RNAG-BOHB		HNAG-BOHB	
	Accuracy	Cost	Accuracy	Cost
CIFAR10	93.5	14.0	95.6	12.8
CIFAR100	72.2	11.8	77.2	10.4
SPORT8	94.7	23.4	95.3	17.6
MIT67	67.7	22.6	71.8	20.0
FLOWERS102	91.4	11.2	93.3	10.6

in our search space as some of them result in architectures which are both efficient and accurate. This justifies our motivation for performing MOBO.

4.2. BO Results

BOHB is used to find the optimal network generator hyperparameters in terms of the validation accuracy. We perform BOHB for 60 iterations with $\eta = 2$. We use training budgets of 100, 200, 400 epochs to evaluate architectures on SPORT8 and 30, 60, 120 epochs on the other datasets.

MOBO returns the Pareto front of generator hyperparameters for two objectives: validation accuracy and sample memory. For parallel MOBO, we start with 50 BOHB evaluation data and search for 30 iterations with a BO batch size of 8. At each BO iteration, the algorithm recommends 8 new points to be evaluated and updates the surrogate model with these new evaluations. We use a fixed training budget of 200 epochs to evaluate architectures suggested for SPORT8 and 60 epochs for the other datasets.

For experiments with both BO methods, we only sample 1 architecture to evaluate the performance of a specific generator. We scale the batch size up to a maximum of 512 to fully utilise the GPU memory and adjust the initial learning rate via linear extrapolation from 0.025 for a batch size of 96 to 0.1 for a batch size of 512. The other network training set-up follows the complete training protocol.

The validation accuracy of the best generator configuration recommended by BOHB as well as the computation costs to complete the BOHB search for both our proposed hierarchical network generator (HNAG) and the Randomly Wired Networks Generator (RNAG) are shown in Table 2. HNAG improves over RNAG in terms of both accuracy and cost.

The query data by MOBO over the two objectives, validation error and sample memory consumption are presented in Figure 3. It shows clearly that the Pareto front of HNAG dominates that of RNAG, showing that our proposed search space not only contains better performing network genera-

Table 3. Generator hyperparameters of the best found models, for single-objective (BOHB; top block) and multi-objective (MOBO; bottom block) experiments. “MPS” is Memory Per Sample.

	Top			Mid		Bottom			MPS (MB)
	N	K	P	N	P	N	K	P	
CIFAR10	8	5	0.6	1	0.7	5	4	0.2	17
CIFAR100	8	5	0.4	1	0.7	4	2	0.4	14
SPORT8	7	2	0.9	5	0.8	6	3	0.6	121
MIT67	9	4	0.6	1	0.2	3	2	0.5	54
FLOWERS102	6	4	0.4	1	0.4	6	5	0.9	62
IMAGENET	4	2	0.5	5	0.6	6	4	0.4	136
CIFAR10	6	4	0.8	1	0.1	3	2	0.5	13
CIFAR100	6	4	0.3	1	0.7	3	2	0.5	13
SPORT8	3	2	0.3	1	0.2	3	2	0.8	43
MIT67	3	2	0.6	1	0.8	4	2	0.6	48
FLOWERS102	6	5	0.2	1	0.8	3	2	0.5	48

tors but also more memory efficient ones.

4.3. Analysis of the Optimal Hyperparameters

Most optimal generators have much fewer nodes (≤ 40 nodes) than the graph-based generator in [Xie et al. \(2019\)](#) (96 nodes) while still achieve better performance as shown in Section 4.4. This shows that the hierarchical design of our search space helps reduce the complexity/size of the architectures found. Interestingly, most datasets have the optimal solution with a single-node mid-level graph. We hypothesize this to be due to the low parameter count we enforced, which encourages the search to be conservative with the total number of nodes. Moreover, we see similar configurations appear to be optimal for different datasets, showing the promise of using transfer-learning to speed up the search in our future work.

4.4. Complete Training Results

We train (i) the best network generator hyperparameters of both HNAG and RNAG found by BO; (ii) the default optimal RNAG setting (RNAG-D) recommended in [Xie et al. \(2019\)](#); and (iii) randomly sampled hyperparameters values for our HNAG (HNAG-RS) following the complete training protocol. HNAG clearly outperforms RNAG (Table 4). Moreover, in the multi-objective case, HNAG-MOBO is able to find models which are not only competitive in test accuracy but also very lightweight (i.e., consuming only 1/3 of the memory when compared to RNAG-D).

An interesting analysis is presented in Figure 4. This plot shows the relationship between randomly-sampled and method-provided architectures, and is thus able to separate the contribution of the search space from that of the search algorithm. Notably, not only does NAGO provide high accuracy, but also has the best relative improvements of all methods. It must be noted that while these methods train their networks using Cutout ([DeVries & Taylor,](#)

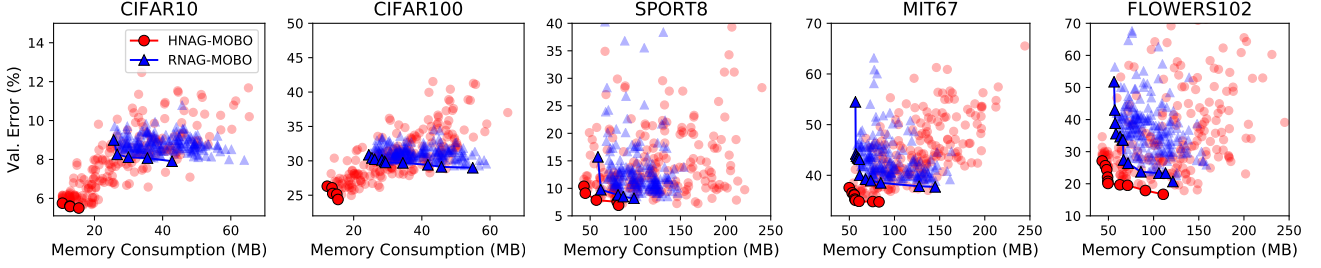


Figure 3. Query data by MOBO for HNAG (red) and RNAG (blue). The Pareto optimal configurations are highlighted in solid lines and filled markers. Each BO evaluation uses 200 training epochs for SPORT8 and 60 training epochs for the other datasets.

Table 4. Test accuracy (%) and memory consumption (MB) achieved by variants of HNAG and RNAG after completing training. “BOHB” and “MOBO” indicates the BO strategy used to find the optimal generator hyperparameters. “RNAG-D” is the best generator configuration recommended in Xie et al. (2019) and “HNAG-RS” means generator hyperparameters are randomly sampled from our search space. In each table entry we show “mean (standard deviation)” of test accuracy (top row) and memory consumption (bottom row). The best performance, separately for test accuracy and memory consumption, is highlighted in bold. Number of model parameters is limited to 4M for CIFAR10 and CIFAR100 and 6M for the other datasets.

	RNAG-BOHB	HNAG-BOHB	RNAG-MOBO	HNAG-MOBO	RNAG-D	HNAG-RS
CIFAR10	94.3(0.13)	96.6(0.15)	94.0(0.26)	96.6(0.07)	94.1(0.16)	95.7(0.68)
	57.9(0.52)	17.0(1.76)	25.9(0.91)	12.8(0.00)	44.2(1.29)	53.9(40.6)
CIFAR100	73.0(0.50)	79.3(0.31)	71.8(0.50)	77.6(0.45)	71.7(0.36)	77.1(1.34)
	56.5(0.90)	14.0(1.07)	27.0(0.91)	12.8(0.00)	43.5(1.23)	72.6(40.2)
SPORT8	93.6(0.76)	94.9(0.52)	93.1(0.73)	95.2(0.40)	93.6(0.99)	93.2(1.55)
	101.9(1.18)	121.9(13.1)	57.8(1.07)	43.1(0.00)	112.1(3.45)	375.7(277)
MIT67	68.3(0.78)	74.2(0.67)	66.9(1.46)	73.5(0.56)	66.7(0.54)	72.5(1.38)
	156.1(6.40)	54.1(2.50)	56.7(0.59)	48.1(0.00)	111.7(3.58)	324.8(140)
FLOWERS102	95.7(0.38)	97.9(0.18)	94.9(0.53)	98.1(0.19)	94.7(0.46)	72.5(1.38)
	143.5(2.27)	61.7(0.00)	63.0(1.63)	48.4(0.00)	111.6(3.35)	324.8(140)

2017), DropPath (Larsson et al., 2016) and Auxiliary Towers (Szegedy et al., 2015), we only used Cutout. DropPath and Auxiliary Towers could conceivably be used with our search space, although an effective and efficient implementation is non-trivial. Furthermore, while the number of parameters in other methods can vary quite a lot (the number of channels is fixed, regardless of the specific solution), NAGO dynamically computes the appropriate number of channels to preserve the given parameter count.

We also perform the search on IMAGENET. Due to resource constraints, we only run 5 iterations of BOHB with search budgets of 15, 30, 60 epochs and train 2 sample networks from the best generator hyperparameters recommended by BOHB, following the complete training protocol in Xie et al. (2019). Although this is likely a sub-optimal configuration, it serves to validate our approach on large datasets such as IMAGENET. The mean network performance achieved by HNAG-BOHB approach outperforms Xie et al. (2019) and other benchmarks (Table 5). Note that XNAS uses DropPath, Auxiliary Towers and AutoAugment (Cubuk et al., 2018) to boost performance.

5. Discussion

Computational cost. While NAGO requires a reasonable amount of time (≤ 20 GPU days), it is slower than some existing methods, which take < 2 GPU days. These works, belonging to the family of one-shot NAS which uses weight-sharing, are able to quickly find good architectures, but to do so their search space needs to be restricted to a fixed macro-structure. It is a trade-off between speed and expressiveness: NAGO’s strength lies in its wide search space. Moreover, NAGO could easily update its surrogate function and output a new optimal architectures in very few samples. For future work it would be interesting to consider a lifelong NAS setting or transfer learning, in which each new task can build on previous experience so that we can quickly get good results on large datasets, such as ImageNet.

Performance. While the results shown are extremely competitive, they are not always the absolute best. This is expected, as we are not leveraging any existing backbone and are instead proposing a completely new one for which it will take time to learn the optimal training strategies. For

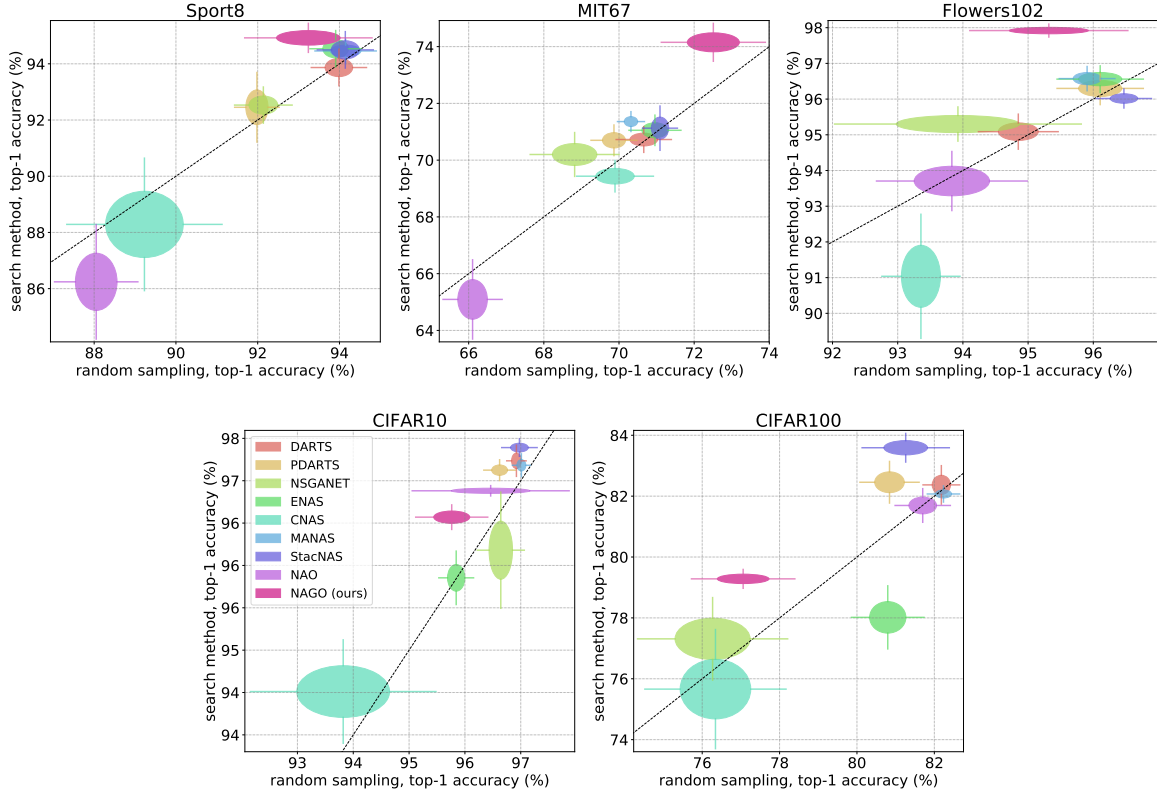


Figure 4. Comparison of search methods and random sampling from their respective search spaces. Ellipse centres, ellipse edges and whisker ends represent the $\mu \pm \{0, \sigma/2, \sigma\}$, respectively (mean μ , standard deviation σ). Methods above the diagonal line outperform the average architecture, and vice-versa. Results for all methods except ours (NAGO: HNAG-BOHB) were taken from public resources provided by Yang et al. (2020). While all high-performing competing methods use Cutout, DropPath and Auxiliary Towers, our method only uses Cutout. The other methods are: DARTS (Liu et al., 2019), PDARTS (Chen et al., 2019), NSGANET (Lu et al., 2019), ENAS (Pham et al., 2018), CNAS (Weng et al., 2019), MANAS (Carlucci et al., 2019), StacNAS (Li et al., 2019), NAO (Luo et al., 2018).

instance, our results do not use DropPath, nor Auxiliary towers, which have been proved to significantly boost performance (Yang et al., 2020). In future work we will aim to transfer existing training protocols to our HNAG backbone.

Interpretability. The network generator hyperparameters define the global properties of the architectures it generates—type and density of connections and operations—and from these we can derive a high level understanding of the properties that make up a good architecture for a given task.

6. Conclusions

We presented NAGO, a novel solution to the NAS problem. Thanks to its highly-expressive hierarchical, graph-based search space, together with its focus on optimizing a generator instead of a specific network, it significantly simplifies the search space and enables the use of a global optimisation strategy. Furthermore, by applying multi-fidelity and multi-objective Bayesian Optimization in our work, we

demonstrated the effectiveness of NAGO on a variety of image tasks and search settings. As such, we believe NAGO offers promising new directions for NAS research.

Table 5. Test accuracy (%) of small networks ($\sim 6M$ parameters) on IMAGENET. We train our HNAG-BOHB for 250 epochs similar to RandomWire-WS (Xie et al., 2019). Other methods are ShuffleNetV2 (Ma et al., 2018), NASNet (Zoph et al., 2018), Amoeba (Real et al., 2019), PNAS (Liu et al., 2018), DARTS (Liu et al., 2019) and XNAS (Nayman et al., 2019).

Network	Top-1 acc.	Top-5 acc.	Params(M)
ShuffleNetV2	74.9	92.2	7.4
NASNet	74.0	91.6	5.3
Amoeba	75.7	92.4	6.4
PNAS	74.2	91.9	5.1
DARTS	73.1	91.0	4.9
XNAS	76.0	—	5.2
RandWire-WS	74.7	92.2	5.6
HNAG-BOHB	76.8	93.4	5.7

References

Alvi, A. S., Ru, B., Calliess, J., Roberts, S. J., and Osborne, M. A. Asynchronous batch Bayesian optimisation with improved local penalisation. *arXiv:1901.10452*, 2019.

Belakaria, S., Deshwal, A., Jayakodi, N. K., and Doppa, J. R. Uncertainty-aware search framework for multi-objective Bayesian optimization. In *Conference on Artificial Intelligence (AAAI)*, 2020.

Bergstra, J., Yamins, D., and Cox, D. D. Making a science of model search: Hyperparameter optimization in hundreds of dimensions for vision architectures. In *International Conference on Machine Learning (ICML)*, 2013.

Bergstra, J. S., Bardenet, R., Bengio, Y., and Kégl, B. Algorithms for hyper-parameter optimization. In *Advances in Neural Information Processing Systems (NIPS)*, pp. 2546–2554, 2011.

Brochu, E., Cora, V. M., and De Freitas, N. A tutorial on bayesian optimization of expensive cost functions, with application to active user modeling and hierarchical reinforcement learning. *arXiv preprint arXiv:1012.2599*, 2010.

Cai, H., Zhu, L., and Han, S. ProxylessNAS: Direct neural architecture search on target task and hardware. In *International Conference on Learning Representations (ICLR)*, 2019.

Carlucci, F., Esperança, P. M., Singh, M., Yang, A., Gabilion, V., Xu, H., Chen, Z., and Wang, J. MANAS: Multi-agent neural architecture search. *arxiv:1909.01051*, 2019.

Chen, X., Xie, L., Wu, J., and Tian, Q. Progressive differentiable architecture search. In *International Conference on Computer Vision (ICCV)*, 2019.

Chen, Y., Huang, A., Wang, Z., Antonoglou, I., Schrittwieser, J., Silver, D., and de Freitas, N. Bayesian optimization in AlphaGo. *arXiv:1812.06855*, 2018.

Cubuk, E. D., Zoph, B., Mane, D., Vasudevan, V., and Le, Q. V. Autoaugment: Learning augmentation policies from data. *arXiv:1805.09501*, 2018.

Deng, J., Dong, W., Socher, R., Li, L.-J., Li, K., and Fei-Fei, L. ImageNet: A large-scale hierarchical image database. In *Computer Vision and Pattern Recognition (CVPR)*, pp. 248–255, 2009.

DeVries, T. and Taylor, G. W. Improved regularization of convolutional neural networks with cutout. *arXiv:1708.04552*, 2017.

Elsken, T., Metzen, J. H., and Hutter, F. Neural architecture search: A survey. *arXiv:1808.05377*, 2018.

Falkner, S., Klein, A., and Hutter, F. BOHB: Robust and efficient hyperparameter optimization at scale. In *International Conference on Machine Learning (ICML)*, pp. 1436–1445, 2018.

Fang, J., Sun, Y., Peng, K., Zhang, Q., Li, Y., Liu, W., and Wang, X. Fast neural network adaptation via parameter remapping and architecture search. In *International Conference on Learning Representations (ICLR)*, 2020.

González, J., Dai, Z., Hennig, P., and Lawrence, N. Batch bayesian optimization via local penalization. In *Artificial Intelligence and Statistics (AISTATS)*, pp. 648–657, 2016.

He, K., Zhang, X., Ren, S., and Sun, J. Deep residual learning for image recognition. In *Computer Vision and Pattern Recognition (CVPR)*, pp. 770–778, 2016.

Hennig, P., Osborne, M. A., and Girolami, M. Probabilistic numerics and uncertainty in computations. *Proc. R. Soc. A*, 471(2179):20150142, 2015.

Huang, G., Liu, Z., Van Der Maaten, L., and Weinberger, K. Q. Densely connected convolutional networks. In *Computer Vision and Pattern Recognition (CVPR)*, pp. 4700–4708, 2017.

Hutter, F., Hoos, H. H., and Leyton-Brown, K. Sequential model-based optimization for general algorithm configuration. In *Learning and Intelligent Optimization (LION)*, pp. 507–523, 2011.

Kandasamy, K., Neiswanger, W., Schneider, J., Poczos, B., and Xing, E. P. Neural architecture search with Bayesian optimisation and optimal transport. In *Advances in Neural Information Processing Systems (NIPS)*, pp. 2016–2025, 2018.

Klein, A., Falkner, S., Bartels, S., Hennig, P., and Hutter, F. Fast Bayesian optimization of machine learning hyperparameters on large datasets. *arXiv:1605.07079*, 2016.

Krizhevsky, A. Learning multiple layers of features from tiny images. Technical report, University of Toronto, 2009.

Larsson, G., Maire, M., and Shakhnarovich, G. Fractalnet: Ultra-deep neural networks without residuals. *arXiv:1605.07648*, 2016.

Li, G., Zhang, X., Wang, Z., Li, Z., and Zhang, T. StacNAS: Towards stable and consistent optimization for differentiable neural architecture search. *arXiv:1909.11926*, 2019.

Li, L.-J. and Fei-Fei, L. What, where and who? classifying events by scene and object recognition. In *International Conference on Computer Vision (ICCV)*, pp. 1–8, 2007.

Liu, C., Zoph, B., Neumann, M., Shlens, J., Hua, W., Li, L.-J., Fei-Fei, L., Yuille, A., Huang, J., and Murphy, K. Progressive neural architecture search. In *European Conference on Computer Vision (ECCV)*, pp. 19–34, 2018.

Liu, H., Simonyan, K., and Yang, Y. DARTS: Differentiable architecture search. In *International Conference on Learning Representations (ICLR)*, 2019.

Lu, Z., Whalen, I., Boddeti, V., Dhebar, Y., Deb, K., Goodman, E., and Banzhaf, W. NSGA-NET: a multi-objective genetic algorithm for neural architecture search. In *Genetic and Evolutionary Computation Conference (GECCO)*, 2019.

Luo, R., Tian, F., Qin, T., Chen, E., and Liu, T.-Y. Neural architecture optimization. In *Advances in Neural Information Processing Systems (NIPS)*, pp. 7816–7827, 2018.

Ma, L., Cui, J., and Yang, B. Deep neural architecture search with deep graph Bayesian optimization. In *Web Intelligence (WI)*, pp. 500–507. IEEE/WIC/ACM, 2019.

Ma, N., Zhang, X., Zheng, H.-T., and Sun, J. Shufflenet v2: Practical guidelines for efficient cnn architecture design. In *Proceedings of the European Conference on Computer Vision (ECCV)*, pp. 116–131, 2018.

Mei, J., Lian, X., Jin, X., Yang, L., Li, Y., Yuille, A., and Yang, J. AtomNAS: Fine-grained end-to-end neural architecture search. In *International Conference on Learning Representations (ICLR)*, 2020.

Nayman, N., Noy, A., Ridnik, T., Friedman, I., Jin, R., and Zelnik, L. XNAS: Neural architecture search with expert advice. In *Advances in Neural Information Processing Systems (NIPS)*, pp. 1975–1985, 2019.

Nilsback, M.-E. and Zisserman, A. Automated flower classification over a large number of classes. In *Indian Conference on Computer Vision, Graphics & Image Processing (ICVGIP)*, pp. 722–729, 2008.

Pham, H., Guan, M., Zoph, B., Le, Q., and Dean, J. Efficient neural architecture search via parameter sharing. In *International Conference on Machine Learning (ICML)*, pp. 4092–4101, 2018.

Quattoni, A. and Torralba, A. Recognizing indoor scenes. In *Computer Vision and Pattern Recognition (CVPR)*, pp. 413–420, 2009.

Real, E., Moore, S., Selle, A., Saxena, S., Suematsu, Y. L., Tan, J., Le, Q. V., and Kurakin, A. Large-scale evolution of image classifiers. In *International Conference on Machine Learning (ICML)*, pp. 2902–2911, 2017.

Real, E., Aggarwal, A., Huang, Y., and Le, Q. V. Regularized evolution for image classifier architecture search. In *Proceedings of the aaai conference on artificial intelligence*, volume 33, pp. 4780–4789, 2019.

Shahriari, B., Swersky, K., Wang, Z., Adams, R. P., and De Freitas, N. Taking the human out of the loop: A review of bayesian optimization. *Proceedings of the IEEE*, 104(1):148–175, 2015.

Shi, H., Pi, R., Xu, H., Li, Z., Kwok, J. T., and Zhang, T. Multi-objective neural architecture search via predictive network performance optimization, 2019.

Snoek, J., Larochelle, H., and Adams, R. P. Practical Bayesian optimization of machine learning algorithms. In *Advances in Neural Information Processing Systems (NIPS)*, pp. 2951–2959, 2012.

Springenberg, J. T., Klein, A., Falkner, S., and Hutter, F. Bayesian optimization with robust Bayesian neural networks. In *Advances in Neural Information Processing Systems (NIPS)*, pp. 4134–4142, 2016.

Szegedy, C., Liu, W., Jia, Y., Sermanet, P., Reed, S., Anguelov, D., Erhan, D., Vanhoucke, V., and Rabinovich, A. Going deeper with convolutions. In *Computer Vision and Pattern Recognition (CVPR)*, pp. 1–9, 2015.

Szegedy, C., Ioffe, S., Vanhoucke, V., and Alemi, A. A. Inception-v4, Inception-ResNet and the impact of residual connections on learning. In *Conference on Artificial Intelligence (AAAI)*, 2017.

Weng, Y., Zhou, T., Liu, L., and Xia, C. Automatic convolutional neural architecture search for image classification under different scenes. *IEEE Access*, 7:38495–38506, 2019.

White, C., Neiswanger, W., and Savani, Y. BANANAS: Bayesian optimization with neural architectures for neural architecture search. *arXiv:1910.11858*, 2019.

Wortsman, M., Farhadi, A., and Rastegari, M. Discovering neural wirings. In *Advances in Neural Information Processing Systems (NIPS)*, pp. 2680–2690, 2019.

Xie, S., Kirillov, A., Girshick, R., and He, K. Exploring randomly wired neural networks for image recognition. *arXiv:1904.01569*, 2019.

Yang, A., Esperanza, P. M., and Carlucci, F. M. NAS evaluation is frustratingly hard. In *International Conference on Learning Representations (ICLR)*, 2020.

Ying, C., Klein, A., Christiansen, E., Real, E., Murphy, K., and Hutter, F. NAS-Bench-101: Towards reproducible neural architecture search. In *International Conference on Machine Learning (ICML)*, pp. 7105–7114, 2019.

Yuan, K., Li, Q., Zhou, Y., Shao, J., and Yan, J. Diving into optimization of topology in neural networks. OpenReview ID:HyetFnEFDS, 2020.

Zabinsky, Z. B. Random search algorithms. *Wiley encyclopedia of operations research and management science*, 2010.

Zoph, B. and Le, Q. Neural architecture search with reinforcement learning. In *International Conference on Learning Representations (ICLR)*, 2017.

Zoph, B., Vasudevan, V., Shlens, J., and Le, Q. V. Learning transferable architectures for scalable image recognition. In *Computer Vision and Pattern Recognition (CVPR)*, pp. 8697–8710, 2018.

A. Quantifying the expressiveness of the hierarchical search space (HNAG)

The total number of possible graphs in our hierarchical search space is larger than

$$T = \underbrace{\left(\sum_{n=3}^{N_O} 2^{\phi(n)} \right)}_{\text{Operation-level}} \cdot \underbrace{\left(\sum_{n=1}^{N_C} 2^{\phi(n)} \right)}_{\text{Cell-level}} \cdot \underbrace{\left(\sum_{n=3}^{N_S} 2^{\phi(n)} \cdot M^n \right)}_{\text{Stage-level}}$$

where $\phi(n) = n(n + 1)/2$ is the number of possible DAGs with n nodes; N_O , N_C , N_S are the maximum numbers of nodes in the operation-, cell- and stage-level graphs, respectively; and M is the number of possible operations in the operation-level graph.

NOTE: This calculation does not include all variations due to the different merging possibilities for each node (addition and concatenation).

Concretely, for the setting implemented ($N_O = N_C = N_S = 10$, $M = 5$) we have $T_{\text{HNAG}} \approx 4.58 \times 10^{56}$. For comparison, the DARTS search space has $T_{\text{DARTS}} = 8^{14} \approx 4.40 \times 10^{12}$.

B. Hyperparameters of the heteroscedastic Bayesian Neural Network Surrogate

Our Bayesian neural network surrogate is a 3-layer fully connected network with 10 neurons for each layer. For sampling network weights, we perform $5 \times |D|$ SGHMC steps as burn-in, followed by 10×100 sampling steps (retaining every 10th sample). We use a total of 100 samples of w_f to approximate the integration in Equation (1) in the main paper. All the other hyperparameters of SGHMC follow the default setting in [Springenberg et al. \(2016\)](#).

C. Local Penalisation for Batch Bayesian Optimization

We adopt the hard local penalization method proposed in [Alvi et al. \(2019\)](#) to collect a batch of new generator configurations which are then evaluated in parallel. The method sequentially selects a batch of B new configurations by repeatedly applying a hard local penalizer function on the selected points (Algorithm 2).

Algorithm 2 Local Penalisation

```

1: Input: BO surrogate model  $p(f|\Theta, D)$  and acquisition
   function  $\alpha(\Theta|D)$ , BO batch size  $B$ , Local penalization
   function  $\phi(\Theta|\Theta^j)$ 
2: Output: The batch of new configurations  $\mathcal{B} =$ 
    $\{\Theta^j\}_{j=1}^B$ 
3:  $\Theta^1 = \arg \max \alpha(\Theta|D)$  and  $\mathcal{B} = \{\Theta^1\}$ 
4: for  $j = 2, \dots, B$  do
5:    $\Theta^j = \arg \max \left( \alpha(\Theta|D) \prod_{i=1}^{j-1} \phi(\Theta|\Theta^i) \right)$ 
6:    $\mathcal{B} \leftarrow \mathcal{B} \cup \Theta^j$ 
7: end for

```

The hard penalisation function is defined as:

$$\phi(\Theta|\Theta^j) = \min \left\{ \frac{L\|\Theta - \Theta^j\|}{|\mu(f|\Theta, D) - M| + \sigma(f|\Theta, D)}, 1 \right\}$$

where M is the best objective value observed so far, $L = \max_{\Theta} \|\nabla \mu(f|\Theta, D)\|$ is the approximated Lipschitz constant of the objective function, and $\mu(f|\Theta, D)$ and $\sigma(f|\Theta, D)$ are predictive posterior mean and standard deviation of the BO surrogate model.

D. Search Range of Generator Hyperparameters

For our Hierarchical Neural Architecture Generator (HNAG), the ranges over which the generator hyperparameters are searched are defined as:

Hyperparameters of the top-level and bottom-level Watts–Strogatz graphs

- The number of nodes in the graph $N_t, N_b \in [3, 10]$
- The number of nearest neighbors to which each node is connected in ring topology $K_t, K_b \in [2, 5]$
- the probability of rewiring each edge $P_t, P_b \in [0.1, 0.9]$

Hyperparameters of the Mid-level Erdős–Rényi graph

- The number of nodes in the graph $N_m \in [1, 10]$
- the probability of edge creation $P_m \in [0.1, 0.9]$

For the Randomly Wired Neural Architecture Generator (RNAG), the hyperparameter ranges are:

Hyperparameters of the Watts–Strogatz graphs in 1st, 2nd and 3rd stages

- The number of nodes in the graph $N_1, N_2, N_3 \in [10, 40]$

- The number of nearest neighbors to which each node is connected in ring topology $K_1, K_2, K_3 \in [2, 9]$
- the probability of rewiring each edge $P_1, P_2, P_3 \in [0.1, 0.9]$

Note that although HNAG has a smaller range for the number of nodes in each graph N than RNAG does, it actually can lead to a much larger range of total number of nodes in an architectures ([9, 1000]) than that of RNAG ([30, 120]).

E. Memory Consumption Range of Architectures from Different Search Space

Our hierarchical graph-based search space can generate architectures with a wider range of memory consumption than those of RNAG and DARTS. We draw 300 sample architectures from the search spaces of HNAG, RNAG and DARTS and evaluate their memory consumption per image. The histogram for results on small-image data and large-image data are shown in Figure 5. It is evident that our proposed search space is much wider than both RNAG and DARTS in terms of the memory consumption.

F. BOHB results on searching more generator hyperparameters

We also perform BOHB on an expanded search space Θ_{expanded} which includes not only the original space of the three random graph model hyperparameters $\Theta_{\text{origin}} = [\theta_{\text{top}}, \theta_{\text{mid}}, \theta_{\text{bottom}}]$ but also hyperparameters controlling the merge options and node operations θ_M and θ_{op} . Specifically, θ_M defines the probability of choosing weighted sum or concatenation when merging multiple inputs at a node. θ_{op} defines the probability of choosing a specific operation among (conv1 \times 1, conv3 \times 3, conv5 \times 5, pool3 \times 3 and pool5 \times 5) for each node in the bottom-level graph. The stage ratio and channel ratio are still fixed to $\theta_S = [0.33, 0.33, 0.33]$ and $\theta_C = [1 : 2 : 4]$ following [Xie et al. \(2019\)](#). Therefore, the expanded search space is

As seen in Table 6, the best validation accuracies achieved by HNAG-Aug-BOHB are lower than that by HNAG-BOHB for all the datasets. This result is counter-intuitive as $\Theta_{\text{origin}} \subset \Theta_{\text{expanded}}$ and thus searching on Θ_{expanded} should lead to better or at least equal performance as on Θ_{origin} . Yet, this result can be explained by the following two reasons:

- 1) the significant increase in optimisation difficulty. The search dimensionality of Θ_{expanded} is almost twice that of Θ_{origin} , which significantly increases the difficulty of BOHB in finding the global optimum⁴. Thus, given similar search budget, BOHB is more likely to find a hyperparameter

⁴To optimize a function to within ϵ distance from the global

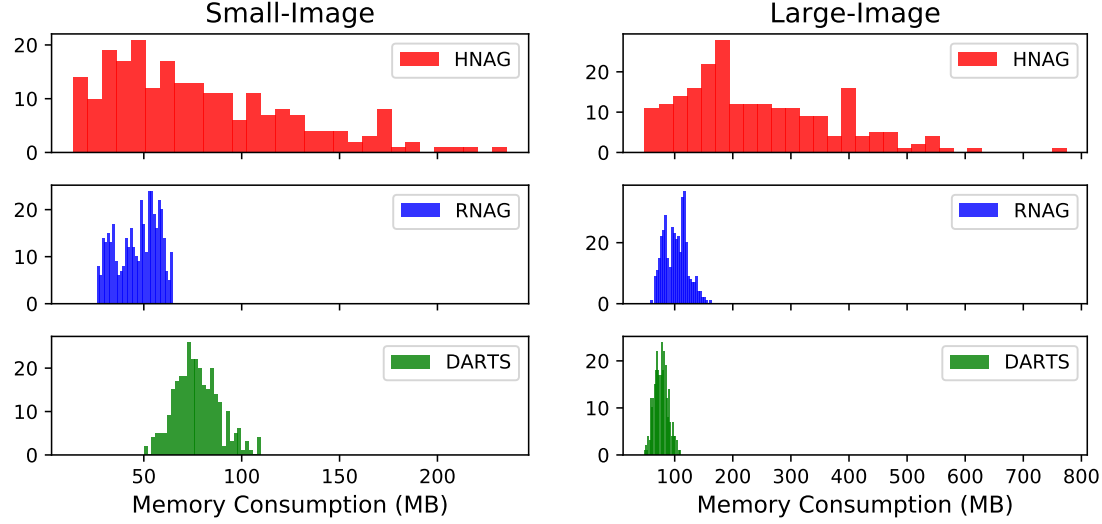


Figure 5. Memory consumption histograms of 300 sample architectures from HNAG, RNAG and DARTS search spaces for small-image $32 \times 32 \times 3$ and large-image $224 \times 224 \times 3$ datasets. Our HNAG search space can generate architectures with a wider range of memory consumption, especially for the large-image data.

ter near the global optimum or a better local optimum in the space Θ_{origin} than in the expanded space $\Theta_{expanded}$.

2) the marginal gain in expanding the search space. Xie et al. (2019) empirically demonstrate that the wiring pattern in a architecture plays a much more important role than the operation choices. Our result in Table 6 confirms this observation; namely, after finding the good wiring, changing the operations only lead to small perturbation on the generator performance. Putting this in the context of generator optimisation, it means that the wiring hyperparameters Θ_{origin} determines the region where the global optimum locates and the hyperparameters controlling the operation and merge options only perturb the exact location of the global optimum to a small extent.

Combing the above two factors, we attribute the worse validation performance for HNAG-Exp-BOHB to the fact that the increase in optimisation difficulty far outweighs the gain in expanding the search space.

G. BOHB samples

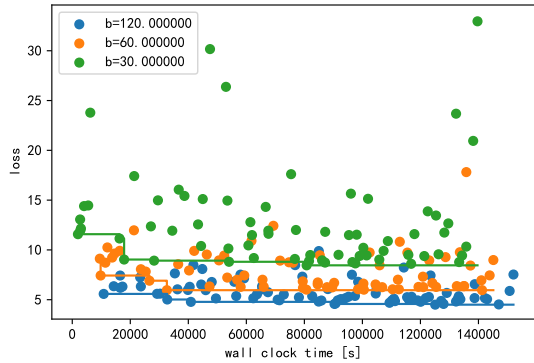
Here we show the BOHB query results on the generator hyperparameters for the case of CIFAR10. We use three training budgets in BOHB: 30 (green), 60 (orange) and 120 (blue) epochs. In Figure 6, the top subplot shows the validation error for the three budgets over time. Query data for different budget are mostly well separated. The bottom subplot shows the spearman rank correlation coefficients

optimum using random search, the expected number of iterations required is $\mathcal{O}(\epsilon^{-d})$ (Zabinsky, 2010)

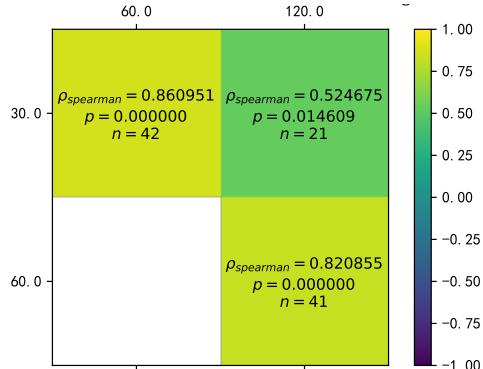
Table 6. Validation accuracy (%) and search cost (GPU days) for BOHB results. The accuracy reported is obtained in the BOHB search setting which uses large batch sizes based on GPU machine memory and trains the network sample for 400 epochs for SPORT8 and 120 epochs for the other datasets. The search space of HNAG-Aug is $\Theta_{expanded} = [\theta_{top}, \theta_{mid}, \theta_{bottom}, \theta_M, \theta_{op}] \in \mathbb{R}^{15}$ while that of HNAG is $\Theta_{origin} = [\theta_{top}, \theta_{mid}, \theta_{bottom}] \in \mathbb{R}^8$.

	HNAG-Exp-BOHB		HNAG-BOHB	
	Accuracy	Cost	Accuracy	Cost
CIFAR10	94.7	19.2	95.6	12.8
CIFAR100	74.5	21.3	77.2	10.4
SPORT8	94.0	26.1	95.3	17.6
MIT67	68.8	33.3	71.8	20.0
FLOWERS102	91.0	14.4	93.3	10.6

$\rho_{spearman} \in [-1, 1]$ of the validation errors between different budgets. It's evident that the $\rho_{spearman}$ between data of 60 epochs and those of 120 epochs are quite high (0.82), indicating that good hyperparameters found in the budget of 60 epochs will remain good when being evaluated with 120 epochs. This motivates our to only a fixed budget of 60 epochs for evaluating all the hyperparameter samples in the multi-objective BO setting.



(a) Validation error for different budgets over time



(b) Rank correlation of validation errors across budgets

Figure 6. BOHB query data across different budgets for HNAG on CIFAR10